Journal of Neural Engineering

High density carbon fiber arrays for chronic electrophysiology, fast scan cyclic voltammetry, and correlative anatomy

To cite this article before publication: Paras R Patel *et al* 2020 *J. Neural Eng.* in press https://doi.org/10.1088/1741-2552/abb1f6

High Density Carbon Fiber Arrays for Chronic Electrophysiology, Fast Scan Cyclic Voltammetry, and Correlative Anatomy

Paras R. Patel[1], Pavlo Popov[2], Ciara M. Caldwell[1], Elissa J. Welle[1], Daniel Egert[3], Jeffrey R. Pettibone[3], Douglas H. Roossien[4], Jill B. Becker[2,5], Joshua D. Berke[3,7], Cynthia A. Chestek[1,8,9,10,*], Dawen Cai[4,6,9,11,*]

[1]Department of Biomedical Engineering, University of Michigan, Ann Arbor, MI 48109, USA
[2]Department of Psychology, University of Michigan, Ann Arbor, MI 48109, USA
[3]Department of Neurology, University of California, San Francisco, CA 94158, USA
[4]Department of Cell and Developmental Biology, University of Michigan Medical School, Ann Arbor, MI 48109, USA
[5]Molecular and Behavioral Neuroscience Institute, University of Michigan, Ann Arbor, MI 48109, USA
[6]Department of Biophysics, University of Michigan, Ann Arbor, MI 48109, USA
[7]Kavli Institute for Fundamental Neuroscience, University of California, San Francisco, CA 94158, USA
[8]Department of Electrical Engineering and Computer Science, University of Michigan, Ann Arbor, MI 48109, USA
[9]Neurosciences Program, University of Michigan, Ann Arbor, MI 48109, USA
[10]Robotics Program, University of Michigan, Ann Arbor, MI 48109, USA
[11]Lead Contact
[*]Co-senior authors and correspondence: cchestek@umich.edu & dwcai@umich.edu

Abstract

Multimodal measurements at the neuronal level allow for detailed insight into local circuit function. However, most behavioral studies focus on one or two modalities and are generally limited by the available technology. Here, we show a combined approach of electrophysiology recordings, chemical sensing, and histological localization of the electrode tips within tissue. The key enabling technology is the underlying use of carbon fiber electrodes, which are small, electrically conductive, and sensitive to dopamine. The carbon fibers were functionalized by coating with Parylene C, a thin insulator with a high dielectric constant, coupled with selective re-exposure of the carbon surface using laser ablation. We demonstrate the use of this technology by implanting 16 channel arrays in the rat nucleus accumbens. Chronic electrophysiology and dopamine signals were detected one month post implant. Additionally, electrodes were left in the tissue, sliced in place during histology, and showed minimal tissue damage. Our results validate our new technology and methods, which will enable a more comprehensive circuit level understanding of the brain.

Keywords

dopamine, slice in place, NeuN, calbindin, nucleus accumbens, neurotransmitter

1. Introduction

To obtain a complete picture of the many potential underlying mechanisms of brain function, it is important to examine multiple modalities during naturally occurring behaviors. One such

modality is neural electrical activity, recorded from a subset of neurons in the brain region of interest. Action potentials are an excellent indicator of information processing at the millisecond timescale and can be well correlated with behavioral variables of interest [1–3]. Coupling this with measurements of neurotransmitters, which are also associated with behavioral variables [4,5], can complement the information gained from neural recordings, providing another modality to better understand brain function. Both modalities are still primarily examined in isolation and information contained within the interaction between the two is usually overlooked, though some progress has been made towards solving this issue [6]. Another important modality is tissue architecture. Typically, electrophysiology data is collected with only a general understanding of the anatomy surrounding the electrode. However, in combining neural recordings with neurotransmitter measurements, it is equally important to understand the cell type and synaptic connections of the neurons immediately surrounding the electrode [7,8].

The state of the art in neurotechnology is to do each of these three things very well in isolation, i.e. in separate animals and usually in separate labs. One technology that can combine two of these modalities together is two photon calcium imaging, which can view spiking activity from a large number of neurons while simultaneously viewing the tissue architecture [9,10]. However, the temporal resolution of firing activity is not as precise as that of traditional penetrating recording electrodes and the imaging depth is limited to approximately one millimeter below the brain surface [11,12]. These challenges would make it difficult to observe long-term trends such as changes in neural plasticity in deeper structures seen during the development of addiction [13].

More typically, modalities such as recording chronic electrophysiology are done in isolation and utilize multi-channel silicon probes that can record from a large number of neurons [14–16]. In recent years, the channel count has increased dramatically for both passive contacts, up to 256 channels in a single array [3,17], and active contacts, with up to 960 multiplexed channels [18]. However, they are limited by their inability to perform chemical sensing. In addition, conventional silicon probes are associated with heavy scarring [19–23] or mechanical failure [24] when chronically implanted. This causes a variety of problems, including a shortened array lifetime [24–26]. It is also unclear if the function of the remaining neurons in the inflammatory region, whether over the course of months or years, is similar to what it would have been in a healthy brain. Finally, the presence of the electrode itself makes it very difficult to image the neural circuitry as probes are typically removed before slicing which severely distorts the tissue.

Carbon fiber electrodes may be well suited to address the challenges in combining all three modalities. Historically, carbon fibers have been used to detect catecholamines using fast scan cyclic voltammetry (FSCV) with a particular focus on dopamine [5,8,27–30]. More recently, they have been used to sense a variety of other neurotransmitters [31,32] including adenosine [33], glutamate [34], and nitric oxide [35]. While previous studies utilized single carbon fibers encapsulated in glass capillaries [27] or fused silica [36], more recent work has led to the development of Parylene C coated carbon fiber arrays capable of dopamine detection in rats [37,38] and primates [39]. The use of Parylene C greatly reduces the footprint of the electrodes thereby causing less damage [40], which has also been validated with chronically implanted carbon fibers that show minimal to non-existent scarring within the implanted brain area [22,37,41]. In addition to chemical sensing, Parylene C coated carbon fiber arrays have been formed that can also detect chronic unit activity [22,42,43]. This is achieved by forming a low impedance surface at the recording site by either exposing a length of the carbon fiber [43,44] or

specifically electroplating materials high surface area materials such as poly(3,4-ethylenedioxythiophene) (PEDOT) [22,45–47]. More recently, it has been shown that single carbon fibers can be coated with nanodiamonds, enabling both electrophysiology and dopamine detection [48]. Adding to the versatility and benefits of carbon fibers are their high Young's modulus and high fracture toughness [41] which enables an array of individuated fibers to self-penetrate the rat pia at lengths of 500 µm to 1000 µm [42,49]. Lastly, owning to their small size, carbon fibers can remain within the tissue during cryosectioning [47] and be localized during imaging as demonstrated by other groups with similarly sized technology [50,51].

In this work, we aim to bridge the divide between the individual benefits of carbon fibers. To do this we will combine them into an array platform that can probe the brain through electrical and chemical detection coupled with elucidating underlying tissue architecture. First, we will show that our new carbon fiber arrays simultaneously have low impedance, which is ideal for detecting unit activity, and second, have high sensitivity to dopamine. Next, we will demonstrate that the arrays can record unit and dopaminergic activity from rat nucleus accumbens. Finally, using our slice-in-place histology technique that allows us to leave the carbon fibers in place during tissue processing, we will precisely localize the position of the fibers within the brain.

2. Materials & Methods

2.1 Device fabrication, preparation, and characterization

2.1.1 Flex array fabrication

One of the carbon fiber devices, or flex array, used in this study was built upon a custom manufactured printed circuit board (PCB) made of 100 µm thick polyimide (MicroConnex, Snoqualmie, WA). A connector (A79024-001, Omnetics, Minneapolis, MN) was soldered on to the top of the flex array and the feet covered with 2-part quick curing epoxy (1FBG8, Grainger, Lake Forest, IL) (figure 1(a)). At the bottom of the flex array, carbon fibers were attached to the exposed traces using silver epoxy (H20E, Epoxy Technology, Billerica, MA) (figure 1(a) red box and figure 1(b)) that was deposited between every other trace, resulting in a pitch of 132 µm (figure 1(c)). A 2-3 mm bare carbon fiber (T-650/35 3K, Cytec Thornel, Woodland Park, NJ) was placed in the silver epoxy using forceps and the epoxy was then oven cured (figure 1(d)). This was repeated on the other side of the flex array, creating a 16 channel array in a 2 x 8 configuration. The exposed trace-silver epoxy-carbon fiber bond was covered in an insulating epoxy (OG142-87, Epoxy Technology, Billerica, MA) and cured with a UV light source (SpotCure-B6, Kinetic Instruments, Limington, MN) (figure 1(e)). Carbon fibers were then cut to 1 mm and coated with approximately 800 nm of Parylene C (PDS 2035, Specialty Coating Systems, Indianapolis, IN). After coating, the carbon fibers were cut down to 500 µm in length (figure 1(f)) and the tips prepared according to **Tip preparation**.

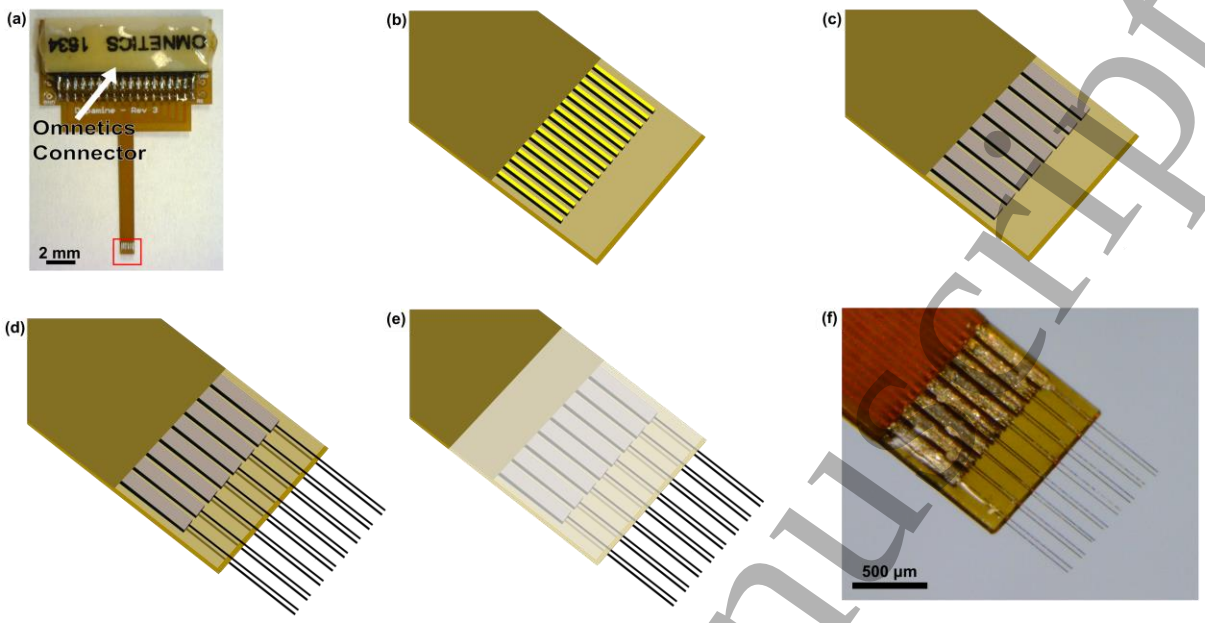

Figure 1. Fabrication of a flex array. (a) Layout of a fully populated flex array with Omnetics connector at the top and carbon fibers at the bottom (red box). (b) Illustration of the bare gold traces at the bottom of an unpopulated flex array. (c) Deposition of silver epoxy between every other trace creates a conductive well for the carbon fibers to rest within. (d) Hand placement of the carbon fibers on both sides of the flex array after which the silver epoxy is oven cured. (e) The exposed trace-silver epoxy-carbon fiber bonds are covered with a UV-cured insulating epoxy. (f) Image of a fully populated flex array with 16 carbon fibers, 8 on each side, at a pitch of 132 µm.

2.1.2 Test array fabrication

Test arrays were fabricated according to a previously published carbon fiber array [22,42]. To begin, a custom PCB was manufactured (Coast to Coast Circuits, Huntington Beach, CA) with 16 exposed traces, 8 on each side of the board, with a pitch of 152 µm. At the top of the PCB a connector (DF30FC-20DS-0.4V, Hirose, Simi Valley, CA) was soldered to each side of the board and covered with a shroud to conform to ZIF interfacing headstages (Tucker Davis Technologies, Alachua, FL). Similar to the flex array fabrication, carbon fibers were mounted to the exposed traces at the bottom of the PCB using silver epoxy (H20E, Epoxy Technology, Billerica, MA), which was then oven cured. The exposed bond was protected with an oven cured insulating epoxy (353NDT, Epoxy Technology, Billerica, MA). Carbon fibers were then cut to 2-3 mm and coated with approximately 800 nm of Parylene C (PDS 2035, Specialty Coating Systems, Indianapolis, IN). After coating, the carbon fiber tips were prepared according to **Tip preparation**.

2.1.3 Tip preparation

To re-expose the underlying surface of the insulated carbon fibers the most distal 50 µm or 100 µm of the fibers was ablated using a 532 nm Karl Suss green laser (energy 5 mJ and pulse duration 5 ns) at a power of 250 and intensity of 100%. The probes were plasma ashed using a Glen 1000P Plasma Cleaner (pressure 200 mT, power 300 W, time 120 seconds, oxygen flow rate 60 sccm, and argon flow rate 7 sccm). Lastly, for the flex arrays, 127 µm diameter silver wires with a 4 µm thick Teflon coating (AGT05100, World Precision Instruments, Sarasota, FL) were soldered to the board for electrophysiology ground and reference connections.

2.1.4 Impedance characterization

Impedance measurements were taken using an Autolab (PGSTAT12, EcoChemie, Utrecht, Netherlands) controlled by vendor provided NOVA software in a 3-electrode configuration. The carbon fibers, reference electrode (RE-5B, BASi, West Lafayette, IN), and stainless steel counter electrode were submerged in 1x phosphate buffered saline (PBS) (BP3994, Fisher, Waltham, MA). Data was obtained by applying a 10 mV_{rms} signal from 10 Hz to 31 kHz and analyzed using custom Matlab 2018a (Mathworks, Natick, MA) scripts.

2.1.5 Dopamine acquisition, flow cell calibration, and analysis

Acquisition of dopaminergic FSCV data was accomplished using a custom setup. Briefly, a headstage, capable of 16 independent channels of simultaneous acquisition, was fabricated using the FSCV circuit described in Takmakov et al., 2011 [52]. One end of the headstage plugged directly into the array and the other end led to a breakout box. The breakout box contained two connector blocks (777145-02, National Instruments, Austin, TX) that interfaced between the headstage and two data acquisition cards (781100-01, National Instruments, Austin, TX). The amplifiers on the headstage were powered by a standalone power supply (1672, BK Precision, Yorba Linda, CA) and chemical reference was provided by a silver | silver chloride (Ag|AgCl) wire. The Ag|AgCl wire was made by connecting the cathode end of a power supply to a silver wire (265586, Sigma, St. Louis, MO) and the anode end to a stainless steel wire. The two wires were placed in 1N hydrochloric acid (S25356, Fisher, Waltham, MA) and 6 V was applied for 20 seconds. All electronic devices were connected to an isolation transformer (IS1000, Tripp Lite, Chicago, IL) to minimize noise. Data was acquired using TarHeelCV [53] for the test arrays and a custom LabVIEW 2018 VI (National Instruments, Austin, TX) for the flex arrays. A complete description of the setup, including parts lists, circuit layout files, build instructions, and software, can be found at mint.engin.umich.edu.

Calibration of all fibers started by reaching a steady baseline current while passing artificial cerebral spinal fluid (aCSF) over the fibers and then applying boluses of dopamine at varying concentrations. The aCSF contained, 125 nM sodium chloride (S271-500, Fisher, Waltham, MA), 1 mM D-(+)-glucose (G7528, Sigma, St. Louis, MO), 4 mM potassium chloride (P217, Fisher, Waltham, MA), 1.3 mM calcium chloride (C1016, Sigma, St. Louis, MO), 1 mM magnesium chloride hexahydrate (M33, Fisher, Waltham, MA), 2 mM sodium phosphate dibasic (S375, Fisher, Waltham, MA), and 0.66 mM sodium phosphate monobasic (S369, Fisher, Waltham, MA) in deionized water which was brought to a final pH of 7.4. The varying concentrations of dopamine started as a stock solution of 0.1 M dopamine hydrochloride (H8502, Sigma, St. Louis, MO) and 0.099 M perchloric acid (A2296, Fisher, Waltham, MA) in deionized water. The stock was then diluted to a concentration of 1000 nM, which then went through serial dilutions to reach concentrations of 500 nM, 250 nM, and 125 nM. Once baseline was reached, the aCSF was turned off, while a given concentration of dopamine was simultaneously turned on. After a ~10 second interval, the dopamine was turned off while simultaneously turning back on the aCSF to allow for a washout and return to baseline. This procedure was repeated three times for each concentration of dopamine.

To determine the current response of each fiber to the different concentrations of dopamine we used the software package TarHeelCV [53] for the test arrays and HDCV Analysis [54] for the flex arrays. For each trial, the background subtracted current was set to a few seconds before the onset of the dopamine bolus. During the current change, due to dopamine oxidation, values were measured at the peak of the onset, just before drop off due to the washout, and in between these two points. All values were obtained by the same operator.

2.2 Chronic electrode implantation

2.2.1 Implantation of flex arrays

To begin Long Evans male rats (Charles River, Wilmington, MA) weighing between 500-650g, were anesthetized with either isoflurane (5% (v/v) for induction and 1-3% (v/v) for maintenance), ketamine/xylazine (100/20 mg/kg), or ketamine/dexmedetomidine (75/0.3 mg/kg). In addition, some animals received 0.1 mL of 2% lidocaine at the proposed incision site and cefazolin (70 mg/mg), while all animals received carprofen (5 mg/kg). After shaving the head, the area was triple swabbed with alternating applications of betadine and 70% ethanol. Ophthalmic ointment was applied to the eyes to prevent drying and a heating pad was used to maintain body temperature.

After making a midline incision and pulling away of the tissue flaps, the following holes, all relative to bregma, were drilled: -4 mm (A/P) and +4 mm left (M/L) for the reference electrode cannula, -5.2 mm (A/P) and +1 mm right (M/L) for the stimulation electrode, and +1.5 mm (A/P) and +1 mm ± 0.85 mm right (M/L) for the flex array's cannula. Next, 4-6 holes at the periphery of the skull were drilled for the bone screws (1ZY93, Grainger, Lake Forest, IL) which were then screwed into place. The reference electrode cannula (MD-2251, BASi, West Lafayette, IN) was then implanted and stopped just at the brain's surface before being cemented in place.

To determine the optimal placement for the stimulation electrode, first a single carbon fiber in a glass cannula was driven in approximately ~6-7 mm, from the top of the skull, into the hole made for the flex array. Next, a 200 µm diameter stainless steel stimulating electrode (C315G-MS303/2/SPC, InVivo1, Roanoke, VA) was driven in ~7 mm (targeting ventral tegmental area) and then slowly advanced while applying a stimulation pulse and simultaneously acquiring FSCV signal from the carbon fiber. Once stimulation induced dopamine was detected on the carbon fiber, the stimulation electrode was cemented in place, the single carbon fiber slowly withdrawn, and the reference wire's cannula's stylet was reinserted.

Next, a custom glass cannula (Vitrocom, Boonton, NJ), ~8 mm in length, was filled with a strip of polyimide that was flush with the implant end of the cannula and protruded from the non-implant end, where they were tacked together using poly(ethylene glycol) (PEG) (295906, Sigma, St. Louis, MO). The strip of polyimide serves two purposes during the insertion process; first, it prevents fluid and tissue from entering the glass cannula and second, it provides a robust surface that can be grasped. After driving in the cannula 6.5 mm, using the skull as the zero point, it was cemented in place and the polyimide strip removed by dissolving the PEG with saline. Next, the flex array was driven in by the exact length of the glass cannula plus 0.5 mm, which ensured that only the fibers on the flex array, also 0.5 mm in length, protruded beyond the cannula (figures 2(a) and 2(b)). The array was then cemented in place, the electrophysiology reference and ground wires attached to a bone screw over the cerebellum, and then the wires were also covered with cement. Additional dental cement was applied as needed. To protect all the devices and to minimize debris from entering the Omnetics connector, the cap of a 50 mL conical tube (14-432-22, Fisher, Waltham, MA), with a hole cut out of the top, was cemented around the implanted devices with the threads facing upward. Then a 1-2 cm portion of the threaded end of the conical tube was screwed into the cap and the exposed end of the tube covered with tape.

Post-operatively, animals were given 1-2 cc of warm saline per 100 g of body weight. Animals recovered on a heated pad placed under their cage. In the days following surgery,

animals were given post-operative carprofen (5 mg/kg) and/or cefazolin (70 mg/kg) as needed based on pain assessment. All procedures and postoperative care complied with the University of Michigan's Institutional Animal Care & Use Committee.

2.2.2 In vivo electrophysiology acquisition and analysis

Neural recordings were acquired using an Intan RHD2000 interface board coupled with an Intan RHD2132 headstage (Intan, Los Angeles, CA). During data acquisition the headstage was set to a band pass range of 0.1 Hz to 7.5 kHz with a sampling rate of 30 kHz. To analyze the data, first, a common average reference signal was subtracted from all recording channels. Next, the data was imported into Offline Sorter (Plexon, Dallas, TX) and high-pass filtered using a 4^{th} order Butterworth filter with a corner frequency of 250 Hz. Lastly, each channel's threshold was manually set and the waveforms sorted by a trained operator.

2.2.3 In vivo dopaminergic recordings, stimulation, and analysis

For each recording session, an Ag|AgCl reference wire was inserted into its designated cannula. The same hardware and software used for calibration was also used for *in vivo* recordings. The acquisition headstage was connected via an external wire to the Ag|AgCl wire using a gold pin interface (82K7797, Newark, Chicago, IL). Data was acquired using a custom LabVIEW VI and analyzed using HDCV Analysis [54] by a trained operator who determined the optimal point to set as the background current.

During stimulation trials a 60 Hz pulse train, with 5 ms monophasic pulses and 135 µA peak amplitude, was applied for 1 second to the implanted stimulation electrode using an isolator unit (ISO-Flex, A.M.P. Instruments, Jerusalem, Israel).

2.3 Histology

2.3.1 Perfusion, skull decalcification, and slice-in-place

Animals were first deeply anesthetized with 5% (v/v) isoflurane before starting a transcardial perfusion of 300-500 mL 1x PBS. This was followed by 300-500 mL of a 4% (w/v) paraformaldehyde (PFA) (19210, Electron Microscope Sciences, Hatfield, PA) solution (pH 7.4-7.5) in 1x PBS. The animal was then decapitated and all tissue removed from the skull. The dental cement headcap was left attached to the skull and remained in place during all subsequent processing steps. Next, the skull was left to sit in 4% PFA at 4 ºC for 24-48 hours. After this time the samples were switched to 0.25 M ethylenediaminetetraacetic acid disodium salt hydrate (EDTA) (E5134, Sigma, St. Louis, MO) (pH 7.4-7.5) in 1x PBS while sitting on a shaker table, also at 4 ºC, at the lowest possible setting (figure 2(c)). The EDTA solution was changed out every 24-48 hours until the skull was fully decalcified, which took approximately 2-4 weeks. To check for full decalcification a razor blade was used to try and slice through the thicker regions of the skull without going so far as to damage the underlying brain. If there was any resistance during the manual slicing the sample was put back for further decalcification.

Once fully decalcified the sample was then soaked in 30% (w/v) sucrose (84097, Sigma, St. Louis, MO) in 1x PBS, at 4 ºC, for at least 72 hours. If after 72 hours the sample had not sunk to the bottom of the container, the solution was changed out and small holes were made near the ear canal to allow for better penetration of the sucrose solution. Before slicing, the skull was carefully trimmed of excess tissue, such as the jaw and cerebellum, and an identifying mark (e.g. a notch) introduced in the hemisphere contralateral to the implant for easier identification and

orientation during imaging. The skull was then placed in a 50:50 mixture of OCT (23-730-625, Fisher, Waltham, MA) and 30% (w/v) sucrose and then put into a vacuum chamber. The chamber was pumped down to -0.06 MPa and kept at this pressure for 20 minutes. The skull was then placed in only OCT and the pumping process repeated for another 20 minutes. Next, the skull was gently wrapped in foil, without wiping off excess OCT, and placed in dry ice for 5 minutes. After freezing, OCT at the very top of the sample (i.e. where the Omnetics connector sticks out of the headcap) was shaved to create a flat surface. This flat surface was then mounted to an OCT covered cryostat chuck and allowed to freeze. Next, the assembly was flipped over into a silicone mold filled with OCT and left to freeze in dry ice for about 5-10 minutes, before trimming away excess OCT.

Once mounted in the cryostat, ~100 µm thick slices of OCT were removed, using a diamond microtome blade (D554D50, Sturkey, Lebanon, PA), until brain tissue became visible. At this point the chuck was adjusted in the medial/lateral direction until the size of both exposed hemispheres was roughly even. After alignment, 300 µm thick sections were taken until we reached the glass cannula at which point slicing was stopped (figure 2(d)). The slice containing the electrode tips was typically visually identifiable by a clustering of small black dots (figure 2(e)). If available, the use of a stereoscope can greatly aid in this process of identifying sections with electrode tips. Slices were stored at 4 ºC in 1x PBS with 0.02% (w/v) sodium azide (DSS24080, Dot Scientific, Burton, MI) until ready for staining (figure 2(f)).

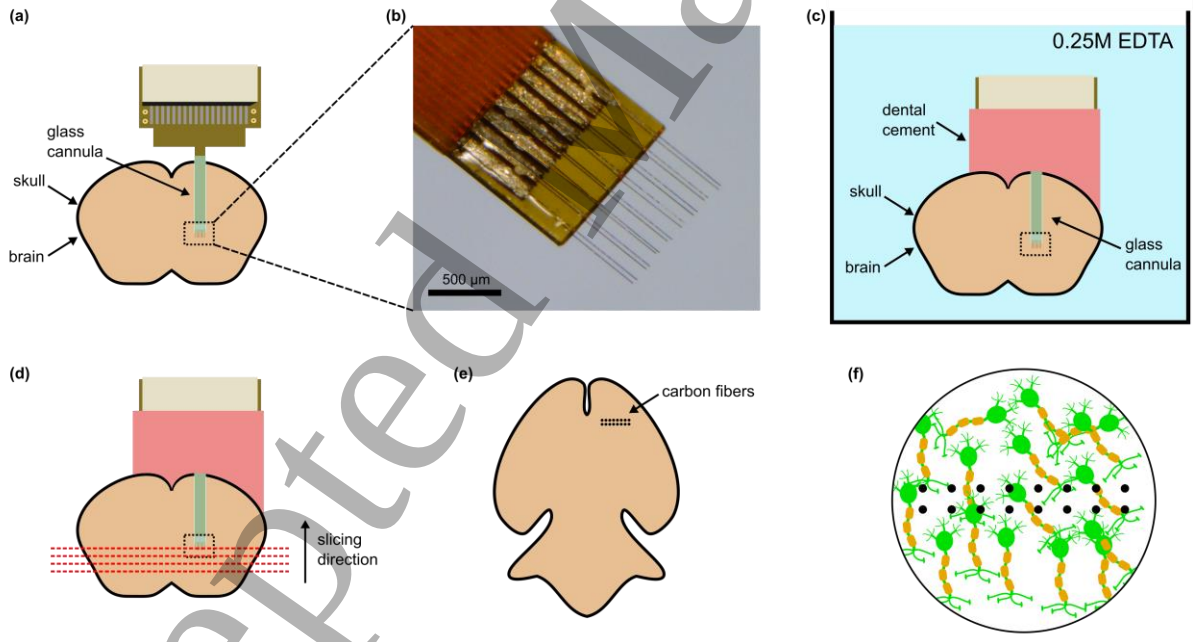

Figure 2. Process flow of slice-in-place technique for a carbon fiber array. (a) The flex array is implanted using a glass cannula as a guide, which is first driven in to just above the target area and then cemented to the skull. (b) Close up of the end of the flex array. Once implanted the carbon fibers extend 500 µm past the end of the glass cannula. (c) At the end of the chronic implant duration, the animal is perfused and decapitated. The skull, brain, and cemented array are kept as one intact unit and placed in EDTA. The EDTA solution is changed every 24-48 hours for 2-4 weeks to decalcify the skull. (d) Once the skull is soft enough for slicing, the sample is cryosectioned in the ventral to dorsal direction until the glass cannula is reached. (e) Visual inspection under a microscope identifies the slice or slices containing the tips of the carbon fibers. (f) Tip containing slices are then stained and imaged to identify the precise carbon fiber tip positions, the cells around the tips, and the brain regions that the tips are located within.

2.3.2 Immunohistochemistry

All steps, unless otherwise noted, took place on a shaker or rotating table set to the lowest possible setting. To begin the staining process slices were further fixed in 4% PFA at 4 ºC for 2 days. Next, the slices were placed in 1x PBS at room temperature (RT) for two hours with a solution change after the first hour. Slices were then placed in starting block (PI37538, Fisher, Waltham, MA) with 1.0% (v/v) triton X-100 (BP151, Fisher, Waltham, MA) at RT, overnight. The next day, slices were triple rinsed in 1x PBS with 0.5% (v/v) triton X-100 (0.5% PBST) at RT, with each rinse lasting one hour. The tissue was then incubated in a primary antibody solution containing mouse anti-Neun (MAB377, 1:250 dilution, Millipore, Burlington, MA) and/or rabbit anti-calbindin (CB-38a, 1:250 dilution, Swant, Marly, Switzerland) in 0.5% PBST with 0.02% azide at 4 ºC for 7-10 days. After incubation, slices were triple rinsed in 1x PBS with 0.5% PBST at RT, with each rinse lasting one hour. Next, the tissue was incubated in a secondary antibody solution containing Alexa 647 donkey anti-mouse IgG (715-605-150, 1:250 dilution, Jackson Labs, Bar Harbor, ME) and/or Alexa 546 donkey anti-rabbit IgG (A10040, 1:250 dilution, Fisher, Waltham, MA) in 0.5% PBST with 0.02% azide at 4 ºC for 3-5 days. The tissue was then rinsed twice in 0.5% PBST at RT, with each rinse lasting two hours.

For one animal the initial primary antibody incubation and subsequent washing step were skipped. At the secondary antibody step the tissue was stained with NeuroTrace 435/455 nissl (N21479, 1:250 dilution, Fisher, Waltham, MA) in 0.5% PBST with 0.02% azide at 4 ºC for 3-5 days. We do not believe that this change in stain impacts our neuron density counts [55].

All samples were stored in 1x PBS with 0.02% azide until ready for imaging.

2.3.3 Imaging & analysis

The day prior to imaging, sections were soaked in increasing concentrations of 2,2'-thiodiethanol (TDE) (88561, Sigma, St. Louis, MO) in 1x PBS at RT, starting with 40% for two hours, then 60% for two hours, 80% for four hours, and finally 100% TDE overnight for refractive index matching. Sections were then imaged on a Zeiss LSM 780 confocal microscope using a 450 nm or 633 nm laser for excitation with a 405 or 488/543/633 dichroic mirror, respectively.

To quantify the neuron population surrounding the implants, images were analyzed using the Fiji distribution of ImageJ 1.49v [56]. First, the perimeter of an electrode/hole was manually identified and a custom macro was run to define concentric rings spaced from 0 µm to 200 µm, in 25 µm increments, away from the defined perimeter. Neurons were counted using the built-in cell counter plugin. All exclusions fell within damage caused by the cannula or white matter tracts.

2.3.4 Statistical analysis

Using IBM SPSS Statistics v24 (IBM Corporation, Armonk, NY) a one-way ANOVA test was used to determine if there existed any difference in neuronal density between any of the radial bin groups, after which a post-hoc Tukey test was used to determine which of the group(s) differed.

3. Results

3.1 Tip preparation optimization for low impedance and high dopamine sensitivity

In order to determine the ideal amount of Parylene C to remove that would result in a low enough impedance for electrophysiology and a high sensitivity to dopamine, characterization tests were performed on a previously published carbon fiber array [22,42] that allowed for higher throughput (see **Methods, Test array fabrication**). The exposed recording site needed to be large enough to achieve a low 1 kHz impedance that would allow for electrophysiological recordings. Previous work has shown that a carbon fiber electrode with only the very tip exposed cannot record unit activity without a surface coating [41]. In addition these coatings, whether optimized for dopamine [57,58] or electrophysiology [22,44], are still susceptible to degradation over time [22,44]. Recent studies have demonstrated that increasing the exposed surface area enables bare carbon fibers to detect unit activity with impedances in the single digit megaohm range [43,44]. To increase the surface area of our electrodes, first the Parylene C coated carbon fibers were laser ablated to re-expose 50 µm or 100 µm of underlying carbon, which led to a 1 kHz impedance in the single digit megaohm range (figure 3(a)). To further reduce impedance, oxygen plasma ashing was applied to the devices and resulted in a decrease in the 1 kHz impedance of both exposure groups (figure 3(a)).

Increasing the surface area to lower impedance has the added benefit of creating more area for dopamine to undergo an oxidation reaction. Using the same test arrays, carbon fibers from the different treatment groups were put into a flow cell chamber and subjected to 1000 nM of dopamine (DA) while an FSCV signal was applied. The resultant current output showed greater sensitivity to dopamine as the surface area increased, coupled with the plasma ashing step (figure 3(b)).

Before choosing a final exposure length, we wanted to confirm that these results still held when using the flex array platform. However, based on these results our group decided that regardless of exposure length, the plasma ashing step was necessary to lower site impedance, while also providing a boost to dopamine sensitivity.

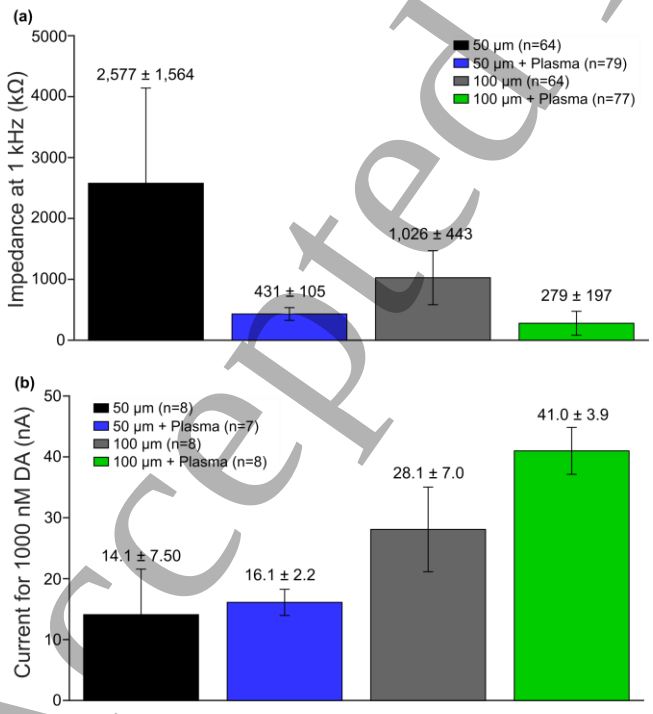

Figure 3. Tip preparation optimization. (a) 1 kHz impedance values (mean ± standard deviation) for different tip treatment groups. The unusually large standard deviation for the 50 µm exposure group is due to one array where 8

out of 16 fibers had abnormally high impedances. All of these fibers were on the same side of the array and the high impedance was possibly the result of an intermittent connection. However, it was difficult to establish an absolute cutoff criterion for bad vs. good fibers, so all data was included. (b) Current response (mean ± standard deviation) of different tip treatment groups to 1000 nM of dopamine during FSCV.

3.2 Flex array impedance and dopamine calibration

We wanted to confirm that the previous electrical impedance and dopamine sensitivity values from the test arrays were maintained when using our flex array platform with carbon fibers of 50 µm or 100 µm exposure lengths, coupled with plasma ashing. Impedance measurements (figure 4(a)) found the 1 kHz values of the 50 µm (370 ± 61 kΩ, n=75 carbon fibers) and 100 µm (225 ± 105 kΩ, n=57 carbon fibers) exposure lengths to be in good agreement with previous results. After completing the fabrication process for the 50 µm exposure group, 75 carbon fibers had sufficiently low impedance, when compared to previous results, out of a possible 80 carbon fibers, for a yield of 94%, while the 100 µm group showed a yield of 89%, with 57 good carbon fibers. Channels were discounted for perceived shorts based on the impedance data where the 1 kHz values of two neighboring carbon fibers was approximately half that of all others. Other channels had too high of an impedance, often exceeding 1 MΩ, and were deemed bad as they did not mirror the results seen with the test arrays.

The flex arrays also underwent dopamine flow cell calibration using concentrations ranging from 125 nM to 1000 nM. Calibration curves for both groups showed a good linear fit (figure 4(b)). Example FSCV false color plots for flex arrays with 50 µm exposure and oxygen plasma, show robust oxidation peaks at both the lowest dopamine concentration (125 nM) for one array (figure 4(c)) and the highest dopamine concentration (1000 nM) for a second array (figure 4(d)). Flow cell results also allow us to determine which additional channels may need to be turned off or discarded as their FSCV plots showed either no response to dopamine or yielded noisy readings (figures 4(c) and 4(d)) during future recordings. Those additional channels that were not originally discounted by impedance measurements contributed to a lower yield (84% for 50 µm and 70% for 100 µm exposure lengths) in the flow cell calibration plots.

Taken together these benchtop tests of impedance and flow cell measurements led us to use the 50 µm exposure length for our *in vivo* testing. At this length we maintain good spatial sensitivity to both local electrochemical and electrophysiological activity.

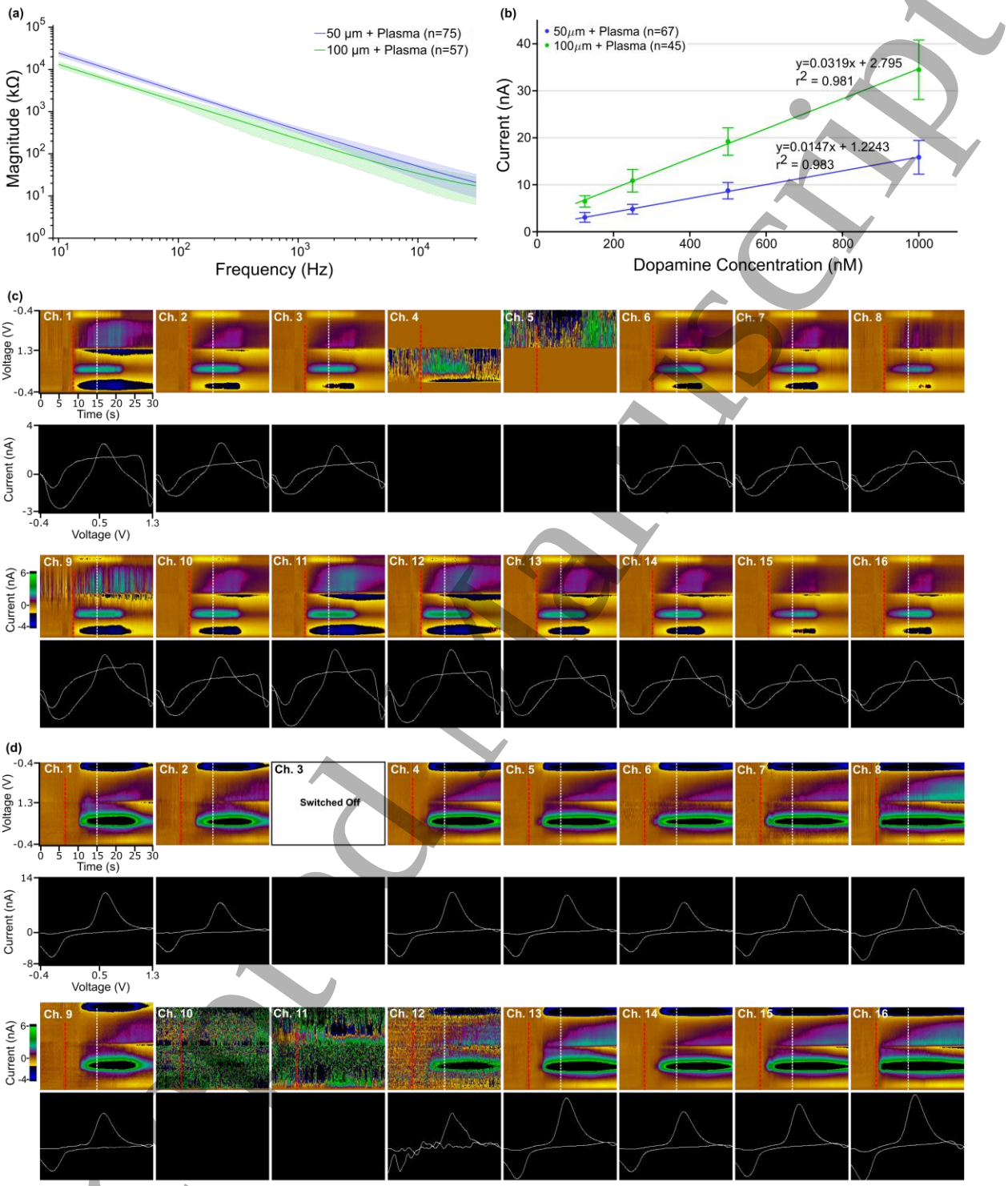

Figure 4. Flex array impedance and dopamine calibration. (a) Average impedance magnitude values (mean ± standard deviation) across a range of frequencies for 50 µm and 100 µm exposure lengths with plasma ashing. (b) Average current response (mean ± standard deviation) to different dopamine concentrations (125 nM, 250 nM, 500 nM, and 1000 nM) for 50 µm and 100 µm exposure lengths with plasma ashing. (c) False color plots and representative voltammograms, taken at 15 sec. (white dashed line), for one array's 16 fibers (50 µm exposure + plasma ashing) subjected to 125 nM of dopamine in flow cell (bolus infusion at red dashed line). Data was collected simultaneously. The plots reveal that channels 4 and 5 did not work and can be ignored during *in vivo* recording

sessions. (d) False color plots and representative voltammograms, taken at 15 sec. (white dashed line), for a second array's 16 fibers (50 µm exposure + plasma ashing) subjected to 1000 nM of dopamine in flow cell (bolus infusion at red dashed line). The slower onset of the oxidation response as compared to the plots in (c) is due to a slower flow rate. Data was collected simultaneously and it can be seen that one channel was turned off pre-emptively and others may need to be turned off as well during *in vivo* recording sessions.

3.3 Neuron density not affected by carbon fibers

To assess potential tissue damage from the implants, histology was performed while leaving the devices in place during the tissue slicing process. During this process the fibers are cut at the same time as the tissue, leaving the fibers embedded within the tissue. They can be easily identified by first using a transmitted light image (figures 5(a) and 5(e)) and followed along the length of the exposed carbon fiber area in fluorescent images of the same tissue stained with NeuN (figures 5(b)-5(d)). In cases where the carbon fibers have fallen out of the tissue during slicing or the post-processing of the tissue, owing to their small size, a tissue hole is still evident in transmitted light images (figures 5(f) and 5(j)) and that hole can also be followed in the z-stack of NeuN images (figures 5(g)-5(i)). To assess any potential volumetric changes in the tissue due to our extended staining times we measured the border of the electrodes/holes (n=14) throughout the depth of the tissue in an animal with an 11.7 week implant (movie S1). An average hole diameter of 8.5 ± 1.8 µm (n=635 measurements) was observed which is comparable to the original carbon fiber plus Parylene C diameter of 8.4 µm. This indicates that our tissue has not undergone major expansion or shrinkage during the two week long staining process.

In a separate four rats, with chronic implants ranging between 10.1-13.3 weeks, histological analysis was performed to observe the neuron density near the electrodes. In these animals 58 electrodes/holes out of the expected 64 were identified and precisely located within a tissue slice. The six unaccounted for carbon fibers most likely were inadvertently broken off during the insertion. In 3 out of 4 animals, the full array extended well past the cannula damage. In the fourth animal, damage from the glass cannula enveloped all but three electrodes. Those three electrodes were included in the analysis as they otherwise appeared to be similar to the others. In total, neuron density was evaluated for 44 identified electrodes/holes, while 14 were discounted due to landing in white matter tracts or being within the cannula's damage radius. Density was calculated by counting the number of neurons within 25 µm bins, starting at the edge of an electrode/hole. Remarkably, the neuron density within about the first 25-100 µm, where the electrodes are most likely to detect units [59], was not significantly different from that at 175-200 µm (figure 5(k)) where the tissue is presumed to have normal neuronal density [19]. The only significant difference was found between the closest and most distant bins (figure 5(k)), but it is important to note that the neuron density within the first 25 µm was still 75% of that at the 175-200 µm distance.

Overall, these results suggest that outside of the cannula damage, our carbon fiber probes lead to minimal damage to the tissue in the area of interest and that we are able to precisely localize our electrodes during histology without explanting the device.

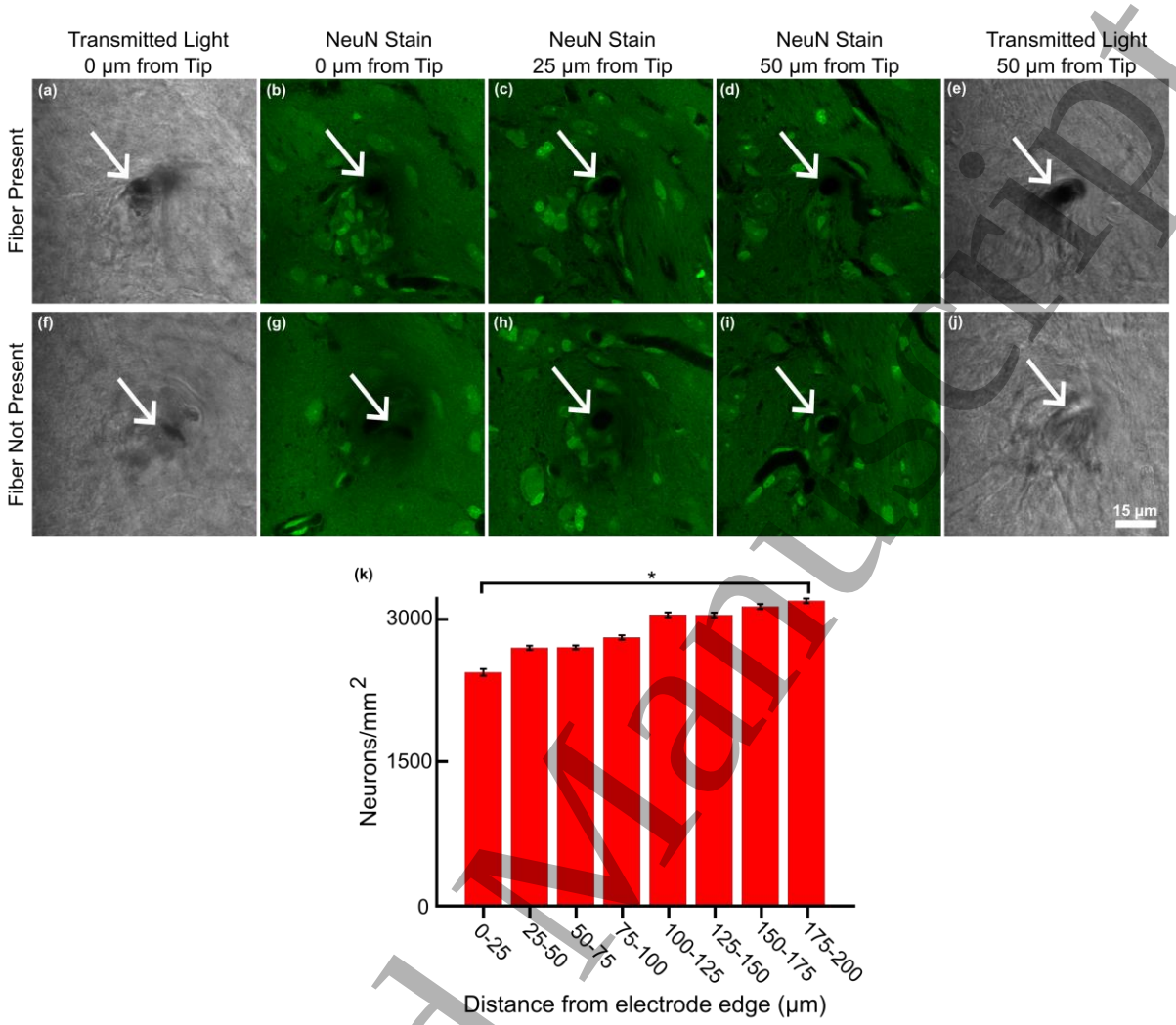

Figure 5. Slice in place histology demonstrates carbon fibers cause no chronic tissue damage. (a) & (e) Transmitted light image of a localized carbon fiber (white arrow) within tissue at the tip (a) and 50 µm from the tip (e). (b)-(d) Successive images of NeuN stained tissue moving away from the tip of the carbon fiber (white arrow) in (a) capturing both the carbon fiber and neighboring neurons. (f) & (j) Transmitted light image of a localized hole (white arrow) that can be detected even if the carbon fiber is not present at the tip (f) and 50 µm from the tip (j). (g)-(i) Successive images of NeuN stained tissue moving away from the tip of the hole (white arrow) in (f) capturing both the hole and neighboring neurons. (k) Calculated neuron density (mean ± standard error) shows no major deficit within the immediate vicinity of the electrodes (n=44), indicating that the carbon fibers do not cause scaring and chronic inflammation. * $p<0.05$.

3.4 Chronic detection of dopaminergic and electrophysiological activity and localization of carbon fibers in vivo

To test the ability of the flex arrays to detect dopaminergic and unit activity *in vivo* we chronically implanted a rat, targeting the nucleus accumbens core and shell regions. At day 15 post-implant, the male rat was paired with a hormonally primed female to elevate natural dopaminergic activity. Stimuli associated with a female rat has been previously shown to induce an increase in dopamine release in male rats [60]. This male rat had not previously been introduced to a female and this interaction produced what we believe to be transient dopamine release detected on 13 channels (figure S1). An important caveat to this initial testing of the array is the lack of control data before and after the introduction of the female. To account for this and

to better test the capability of the array, at day 34 we applied stimulation to the ventral tegmental area (VTA) and saw dopamine detection on 11 channels (figure 6(a)). This also confirms our array implant location in the nucleus accumbens, as the VTA is known to project to nucleus accumbens [61]. On the same day, but in a different session, we were able to detect unit activity on seven channels (insets of figure 6(a)).

At day 78, this animal was sacrificed, perfused, and its tissue sliced with the array in place. In this particular animal the array looks to have landed primarily in the core region with two carbon fibers ending up in the anterior commissure based on a corresponding light image of the entire slice (figures 6(b) and 6(c)). Calbindin staining of the tissue allowed us to verify that the array was primarily implanted in the nucleus accumbens core, with two fibers in the anterior commissure (figure 6(d)). The same tissue section was also stained for NeuN, the carbon fibers identified, and numbered to match their respective recordings channels (figure 6(e)). As seen before, the tissue demonstrates minimal degradation of neuronal health which is not typically found with other electrodes [62]. While carbon fibers 8 and 16 may have partially landed in the anterior commissure, they still detected dopamine under stimulation conditions (figure 6(a)).

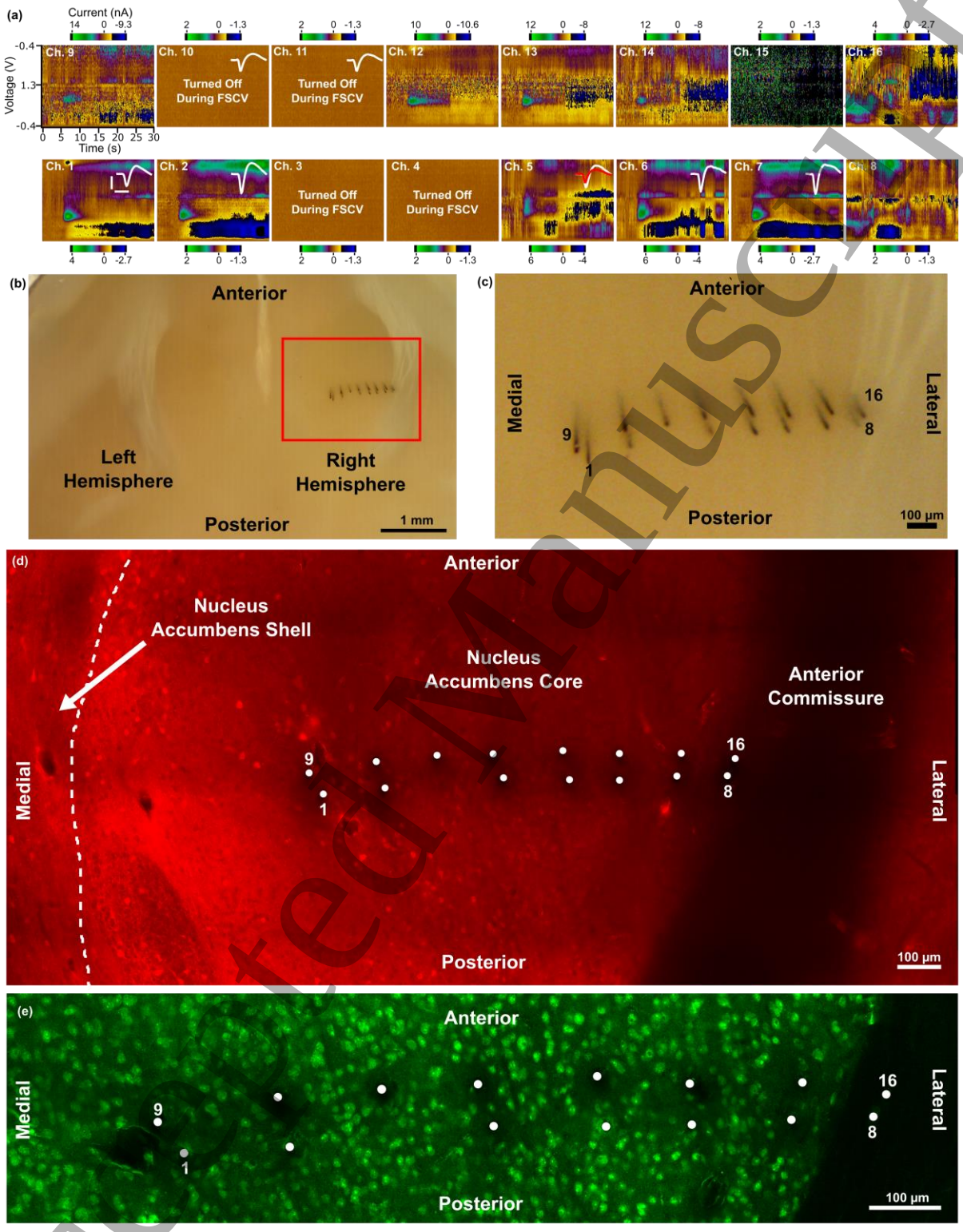

Figure 6. Carbon fiber anatomical localization, tissue response, and chronic detection of dopamine and electrophysiology. (a) Dopamine release detected after stimulation of the VTA (applied at the 5 second mark) on day 34 post-implant. Channel 3 was broken prior to implantation of the array. Insets show detected unit activity in a session after FSCV, using an Intan headstage, on the same day. Horizontal white scale bar is 500 µs and vertical white scale bar is 30 µV. (b) Picture of the carbon fibers (red box) embedded within the tissue after sectioning. (c) Close up from (b) showing the rightmost channels (8 and 16) embedded within the anterior commissure. Individual

carbon fibers have been numbered and correspond to the data shown in (a). (d) Calbindin staining identifies the boundary between the nucleus accumbens core and shell. Here the array's implant location is primarily in the core and partially in the anterior commissure. The white dots indicate the location of the actual carbon fibers, determined using an overlapping transmitted light image (not shown). (e) The same tissue as in (d) but stained with NeuN, showing no obvious damage to the areas immediately surrounding each carbon fiber (white dots).

DISCUSSION

The carbon fiber array presented here represents, to our knowledge, the first array capable of both chronic electrophysiology and chronic chemical sensing which can also be precisely localized within the tissue to identify the recording location.

The chronic electrophysiology and chemical sensing are derived from our unique tip preparation methods. A variety of methods have been used by other groups, including fire-sharpening with a blowtorch [43,63], masking the carbon fibers using photolithography [37], or exposing the ends using cryosectioning [47]. Our laser ablation and plasma ashing approach offers a high degree of flexibility in the amount of carbon that was re-exposed. The laser ablation was critical in re-exposing the underlying carbon and the plasma ashing most likely removed any residual Parylene C, in addition to possible surface roughening. The combination of the two led to low impedances suitable for electrophysiology and high enough dopamine sensitivity to detect dopaminergic signals at one month. While we have not yet implanted a sufficient number of animals to measure chronic longevity of these arrays, others have demonstrated the feasibility of this technology by recording dopaminergic activity from chronically implanted carbon fibers for over a year [38]. In addition, it may be possible in the future to coat our electrode tips with a polymer, such as PEDOT doped with carbon nanotubes [46,64,65], graphene oxide [57], or Nafion [58], to simultaneously improve the fidelity of both recording modalities. Though, additional chronic testing will be necessary to determine if there is any degradation as seen in other PEDOT studies [22,44].

An important aspect to the overall design of this array is that most of the manufacturing steps can be done at the benchtop of most labs. Groups accustomed to handling microwires could learn to handle the placement of carbon fibers within a short time. While the by-hand assembly does increase fabrication time, most steps can be done within 10-15 minutes, with important customization taking place during the process. For example, each individual electrode can be optimized for high quality electrophysiology (with small site size and low impedance coatings such as PEDOT), high quality FSCV (with 100 µm of exposed carbon), or a combination of the two (50 µm exposed, with visible but small spikes). In addition, the circuitry and LabVIEW software used in the present study are available online and can be assembled or modified in-house by any lab. To further the design space, one may consider using fibers made from carbon nanotubes which have a higher surface area than traditional carbon fibers [66,67], leading to increases in dopamine sensitivity. Some of our current yield issues likely stem from silver epoxy accidentally bridging the gap between two sets of traces during fabrication, from fibers breaking during any of the hand fabrication steps, or improper lasering leading to insufficiently exposed area. Regardless of material type or improved tip functionalization [44], improvements to our manufacturing yield and channel count will also be critical in the future. To further this goal, we are currently conducting similar chronic experiments with our carbon fiber + silicon hybrid design [42] which allows for more flexibility in targeting different depths without a glass cannula, easier insertion, faster manufacturing, higher yields, and a better platform for custom configuration.

The ability to slice through our electrodes, determine their precise implant location, and quantify neuronal density can be primarily attributed to the small size of the carbon fibers, which has been seen by other groups with similarly sized electrodes [47,50,51]. We have known for some time that carbon fibers cause very little immune response, but previous studies lacked good neural density metrics because carbon fibers are extremely hard to find when removed due to this minimal scarring [22,41]. For comparison, these electrodes are roughly the size of capillaries found in the cortex [68]. In the present study, we took advantage of this small size to slice the whole array, without apparent movement of any electrodes, and quantify the neuronal density around the electrodes. It is encouraging that 10+ weeks post-implant, the density within the first 100 μm is nearly indistinguishable from normal brain. The lack of damage also suggests future medical applications, such as neuroprosthetics, where stable multi-year recordings are desirable for brain machine interfaces [69]. Finally, the very small size and pitch may ultimately enable use of the present device in nerves and ganglia where carbon based devices have already shown the ability to record unit activity [63,70].

While it is feasible for there to be major movement of the electrodes during the softening phase in EDTA or during handling, we do not believe this to be the case. The handling of the sample is kept to a minimum and done so gently and by the more rigid parts when handling is necessary. Micromotion is the more serious concern, but owning to the flexible nature of the carbon fibers we believe they will move with the tissue if the sample is handled properly.

These devices now provide the ability to relate dopamine and electrophysiology signals to surrounding macro- and micro-structure and will be highly valuable for understanding both natural signals related to learning and motivation [71] and the altered signaling produced by drugs of abuse. Dopamine dynamics are known to differ between subregions such as core and shell [72]. They are also thought to vary between micro- and meso-environments as well [7,8], in part as a result of local control of dopamine release by interneurons [73,74]. It is therefore critical to be able to precisely localize recording sites relative to anatomical features across a wide range of spatial scales.

Works that have studied cellular dopamine release and firing dynamics using the separate techniques of microdialysis and electrophysiology [75,76], could possibly benefit from this work by recording both types of signals, in sequence, from the same area with high temporal and spatial resolution. Alternatively two different probes in the same rat could be used, one to detect dopamine cell firing and the other to detect the downstream release of dopamine in the target region.

More generally and of importance to many neuroscience studies, the high neuron density surrounding the probes suggests that we have not yet reached the limit of electrode pitch or channel count as has been demonstrated by other groups who created PEDOT coated carbon fiber arrays for electrophysiology with closer pitch and higher channel counts [47,77]. Carbon fiber arrays are differentiated from high channel count silicon probes with single shanks because they are distributed across more of the brain rather than along a single path. With our particular architecture, the regular spacing of the fibers, which are far less prone to splaying or migration, enables easier matching of electrode recording data with their physical location within the tissue. This may be useful for recording from interconnected circuits, particularly if the focus is to determine the precise position of the electrodes within them. These preliminary results strongly motivate combining chronic recording of electrical and dopaminergic activity with anatomy imaging techniques. In addition to identifying the recorded neurons *in situ*, our techniques will enable characterizing these neurons' molecular identity using immunofluorescence antibody

staining. Combining with circuit labeling tools, our techniques will further permit functionality, anatomy, and connectivity studies in the same animal at single cell resolution. For instance, we may record and identify many afferent interneurons and their connected single efferent pyramidal cell that are labeled by the trans-monosynaptic rabies virus in the cortex [78]. Such an application will allow us to unambiguously study the differential inhibition effect of different interneuron subtypes onto the same target. In another example, we may combine our techniques with the Brainbow tools, which randomly generates many spectrally distinct colors to label neighboring neurons [79,80]. Using proper sample preparation, imaging, and neuronal tracing methods, Brainbow tools permit us to trace densely labeled neurons and reconstruct neural circuits [81–84]. This combination therefore allows for the investigation of local interactions between recorded and surrounding neurons through detailed anatomical mapping. Ultimately, we envision our novel carbon fiber array platform as enabling a new experimental paradigm for chronic behavioral experiments, wherein high density neuronal electrical and/or chemical activities are recorded, after which their molecular identity, morphology, and connectivity are precisely depicted *in situ* by electrode tip-correlated imaging and analysis.

ACKNOWLEDGEMENTS

We would like to thank Joseph Letner and Drs. Pavel Takmakov, Ali Mohebi, and Arif Hamid for assistance with LabVIEW and FSCV headstage designs; Dr. Brandon Aragona for guidance on voltammetry methods; as well as Dr. Khalil Najafi for use of his lab's equipment. We would also like to thank Julianna Richie for array fabrication and testing and Brandon Luma for performing surgeries and data collection. Lastly, we would like to thank Dr. Paul Garris and Brad Smith for their assistance with voltammetry analysis. This work was financially supported by a Michigan Brain Award, the McKnight Foundation, the National Institute of Mental Health (R01MH110932), the National Institute on Drug Abuse (R01DA045783 and R01DA039952), the National Institute of Neurological Disorders and Stroke (U01NS094375), and the National Science Foundation (1707316).

AUTHOR CONTRIBUTIONS

P.R.P., P.P., J.B.B., D.C., J.D.B., and C.A.C. designed the study. P.R.P., C.M.C., E.J.W., and P.P., developed, built, and tested the arrays. P.P. developed the LabVIEW acquisition software. D.E. created and implemented the laser ablation and plasma ashing methods. P.R.P. and P.P. developed the surgical implantation techniques and collected & analyzed the electrophysiology & FSCV data. J.R.P. developed the tissue decalcifying and thick tissue slicing methods. P.P., C.M.C., and D.H.R. performed the tissue processing and staining. C.M.C., D.C., and C.A.C. performed the neuron density analysis. P.R.P., C.M.C., J.B.B., D.C., J.D.B., and C.A.C. wrote the manuscript. E.J.W. provided edits and all authors approved the final manuscript.

DECLARATION OF INTERESTS

The authors declare no competing interests.

REFERENCES

[1] Churchland M M, Cunningham J P, Kaufman M T, Foster J D, Nuyujukian P, Ryu S I and Shenoy K V 2012 Neural population dynamics during reaching *Nature* **487** 51–6

[2] Cohen J Y, Haesler S, Vong L, Lowell B B and Uchida N 2012 Neuron-type-specific signals for reward and punishment in the ventral tegmental area *Nature* **482** 85–8

[3] Berényi A, Somogyvári Z, Nagy A J, Roux L, Long J D, Fujisawa S, Stark E, Leonardo A, Harris T D and Buzsáki G 2014 Large-scale, high-density (up to 512 channels) recording of local circuits in behaving animals *J. Neurophysiol.* **111** 1132–49

[4] Brown H D, McCutcheon J E, Cone J J, Ragozzino M E and Roitman M F 2019 Primary food reward and reward-predictive stimuli evoke different patterns of phasic dopamine signaling throughout the striatum *Eur. J. Neurosci.* **34** 1997–2006

[5] Rebec G V., Christensen J R C, Guerra C and Bardo M T 1997 Regional and temporal differences in real-time dopamine efflux in the nucleus accumbens during free-choice novelty *Brain Res.* **776** 61–7

[6] Parent K L, Hill D F, Crown L M, Wiegand J P, Gies K F, Miller M A, Atcherley C W, Heien M L and Cowen S L 2017 Platform to Enable Combined Measurement of Dopamine and Neural Activity *Anal. Chem.* **89** 2790–9

[7] Brimblecombe K R and Cragg S J 2015 Substance P Weights Striatal Dopamine Transmission Differently within the Striosome-Matrix Axis *J. Neurosci.* **35** 9017

[8] Wightman R M, Heien M L A V, Wassum K M, Sombers L A, Aragona B J, Khan A S, Ariansen J L, Cheer J F, Phillips P E M and Carelli R M 2007 Dopamine release is heterogeneous within microenvironments of the rat nucleus accumbens *Eur. J. Neurosci.* **26** 2046–54

[9] Stosiek C, Garaschuk O, Holthoff K and Konnerth A 2003 In vivo two-photon calcium imaging of neuronal networks *Proc. Natl. Acad. Sci.* **100** 7319–24

[10] Stirman J N, Smith I T, Kudenov M W and Smith S L 2016 Wide field-of-view, multi-region, two-photon imaging of neuronal activity in the mammalian brain *Nat. Biotechnol.* **34** 857–62

[11] Birkner A, Tischbirek C H and Konnerth A 2017 Improved deep two-photon calcium imaging in vivo *Cell Calcium* **64** 29–35

[12] Helmchen F and Denk W 2005 Deep tissue two-photon microscopy *Nat. Methods* **2** 932–40

[13] Berke J D and Hyman S E 2000 Addiction, Dopamine, and the Molecular Mechanisms of Memory *Neuron* **25** 515–32

[14] Bai Q, Wise K D and Anderson D J 2000 A High-Yield Microassembly Structure for Three-Dimensional Microelectrode Arrays *IEEE Trans Biomed Eng* **47** 281–9

[15] Kipke D R, Vetter R J, Williams J C and Hetke J F 2003 Silicon-substrate intracortical microelectrode arrays for long-term recording of neuronal spike activity in cerebral cortex *IEEE Trans. Neural Syst. Rehabil. Eng.* **11** 151–5

[16] Vetter R J, Williams J C, Hetke J F, Nunamaker E A and Kipke D R 2004 Chronic Neural Recording Using Silicon-Substrate Microelectrode Arrays Implanted in Cerebral Cortex *IEEE Trans. Biomed. Eng.* **51** 896–904

[17] Shobe J L, Claar L D, Parhami S, Bakhurin K I and Masmanidis S C 2015 Brain activity mapping at multiple scales with silicon microprobes containing 1,024 electrodes *J. Neurophysiol.* **114** 2043–52

[18] Jun J J, Steinmetz N A, Siegle J H, Denman D J, Bauza M, Barbarits B, Lee A K, Anastassiou C A, Andrei A, Aydın Ç, Barbic M, Blanche T J, Bonin V, Couto J, Dutta B, Gratiy S L, Gutnisky D A, Häusser M, Karsh B, Ledochowitsch P, Lopez C M, Mitelut C, Musa S, Okun M, Pachitariu M, Putzeys J, Rich P D, Rossant C, Sun W, Svoboda K, Carandini M, Harris K D, Koch C, O'Keefe J and Harris T D 2017 Fully integrated silicon probes for high-density recording of neural activity *Nature* **551** 232

[19] Biran R, Martin D C and Tresco P A 2005 Neuronal cell loss accompanies the brain tissue response to chronically implanted silicon microelectrode arrays *Exp Neurol* **195** 115–26

[20] Szarowski D H, Andersen M D, Retterer S, Spence A J, Isaacson M, Craighead H G, Turner J N and Shain W 2003 Brain responses to micro-machined silicon devices *Brain Res.* **983** 23–35

[21] Polikov V S, Tresco P A and Reichert W M 2005 Response of brain tissue to chronically implanted neural electrodes. [Review] [156 refs] *J. Neurosci. Methods* **148** 1–18

[22] Patel P R, Zhang H, Robbins M T, Nofar J B, Marshall S P, Kobylarek M J, Kozai T D Y, Kotov N A and Chestek C A 2016 Chronic in vivo stability assessment of carbon fiber microelectrode arrays *J. Neural Eng.* **13** 066002

[23] Winslow B D, Christensen M B, Yang W K, Solzbacher F and Tresco P A 2010 A comparison of the tissue response to chronically implanted Parylene-C-coated and uncoated planar silicon microelectrode arrays in rat cortex *Biomaterials* **31** 9163–72

[24] Kozai T D Y, Catt K, Li X, Gugel Z V., Olafsson V T, Vazquez A L and Cui X T 2015 Mechanical failure modes of chronically implanted planar silicon-based neural probes for laminar recording *Biomaterials* **37** 25–39

[25] Gaire J, Lee H C, Hilborn N, Ward R, Regan M and Otto K J 2018 The role of inflammation on the functionality of intracortical microelectrodes *J. Neural Eng.* **15** 066027

[26] Chestek C A, Gilja V, Nuyujukian P, Foster J D, Fan J M, Kaufman M T, Churchland M M, Rivera-Alvidrez Z, Cunningham J P, Ryu S I and Shenoy K V. 2011 Long-term stability of neural prosthetic control signals from silicon cortical arrays in rhesus macaque motor cortex *J. Neural Eng.* **8** 045005

[27] Ponchon J L, Cespuglio R, Gonon F, Jouvet M and Pujol J F 1979 Normal Pulse Polarography With Carbon-fiber Electrodes For Invitro and Invivo Determination of Catecholamines *Anal. Chem.* **51** 1483–6

[28] Wightman R M, May L J and Michael A C 1988 Detection of dopamine dynamics in the brain *Anal. Chem.* **60** 769A-779A

[29] Smith A R, Garris P A and Casto J M 2015 Real-time monitoring of electrically evoked catecholamine signals in the songbird striatum using in vivo fast-scan cyclic voltammetry *J. Chem. Neuroanat.* **66–67** 28–39

[30] Rodeberg N T, Sandberg S G, Johnson J A, Phillips P E M and Wightman R M 2017 Hitchhiker's Guide to Voltammetry: Acute and Chronic Electrodes for in Vivo Fast-Scan Cyclic Voltammetry *ACS Chem. Neurosci.* **8** 221–34

[31] Huffman M L and Venton B J 2008 Carbon-Fiber Microelectrodes for In Vivo Applications *Analyst* **134** 18–24

[32] Bucher E S and Wightman R M 2015 Electrochemical Analysis of Neurotransmitters *Annu. Rev. Anal. Chem.* **8** 239–61

[33] Ross A E and Venton B J 2012 Nafion-CNT coated carbon-fiber microelectrodes for enhanced detection of adenosine *Analyst* **137** 3045–51

[34] Oldenziel W H and Westerink B H C 2005 Improving Glutamate Microsensors by Optimizing the Composition of the Redox Hydrogel *Anal. Chem.* **77** 5520–8

[35] Ferreira N R, Ledo A, Frade J G, Gerhardt G A, Laranjinha J and Barbosa R M 2005 Electrochemical measurement of endogenously produced nitric oxide in brain slices using Nafion/o-phenylenediamine modified carbon fiber microelectrodes *Anal. Chim. Acta* **535**

1–7

[36] Clark J J, Sandberg S G, Wanat M J, Gan J O, Horne E A, Hart A S, Akers C A, Parker J G, Willuhn I, Martinez V, Evans S B, Stella N and Phillips P E M 2010 Chronic microsensors for longitudinal, subsecond dopamine detection in behaving animals *Nat. Methods* **7** 126–9

[37] Schwerdt H N, Kim M J, Amemori S, Homma D, Yoshida T, Shimazu H, Yerramreddy H, Karasan E, Langer R, Graybiel A M and Cima M J 2017 Subcellular probes for neurochemical recording from multiple brain sites *Lab Chip* **17** 1104–15

[38] Schwerdt H N, Zhang E, Kim M J, Yoshida T, Stanwicks L, Amemori S, Dagdeviren H E, Langer R, Cima M J and Graybiel A M 2018 Cellular-scale probes enable stable chronic subsecond monitoring of dopamine neurochemicals in a rodent model *Commun. Biol.* **1** 144

[39] Schwerdt H N, Shimazu H, Amemori K, Amemori S, Tierney P L, Gibson D J, Hong S, Yoshida T, Langer R, Cima M J and Graybiel A M 2017 Long-term dopamine neurochemical monitoring in primates *Proc. Natl. Acad. Sci.* **114** 13260

[40] Seymour J P and Kipke D R 2007 Neural probe design for reduced tissue encapsulation in CNS *Biomaterials* **28** 3594–607

[41] Kozai T D Y, Langhals N B, Patel P R, Deng X, Zhang H, Smith K L, Lahann J, Kotov N A and Kipke D R 2012 Ultrasmall implantable composite microelectrodes with bioactive surfaces for chronic neural interfaces *Nat. Mater.* **11** 1065–73

[42] Patel P R, Na K, Zhang H, Kozai T D Y, Kotov N A, Yoon E and Chestek C A 2015 Insertion of linear 8.4 μm diameter 16 channel carbon fiber electrode arrays for single unit recordings *J. Neural Eng.* **12** 046009

[43] Guitchounts G, Markowitz J E, Liberti W A and Gardner T J 2013 A carbon-fiber electrode array for long-term neural recording. *J. Neural Eng.* **10** 046016

[44] Welle E J, Patel P R, Woods J E, Petrossians A, della Valle E, Vega-Medina A, Richie J M, Cai D, Weiland J D and Chestek C A 2020 Ultra-small carbon fiber electrode recording site optimization and improved in vivo chronic recording yield *J. Neural Eng.* **17** 026037

[45] Ludwig K A, Langhals N B, Joseph M D, Richardson-Burns S M, Hendricks J L and Kipke D R 2011 Poly(3,4-ethylenedioxythiophene) (PEDOT) polymer coatings facilitate smaller neural recording electrodes *J. Neural Eng.* **8** 014001

[46] Kozai T D Y, Catt K, Du Z, Na K, Srivannavit O, Haque R U M, Seymour J, Wise K D, Yoon E and Cui X T 2016 Chronic In Vivo evaluation of PEDOT/CNT for stable neural recordings *IEEE Trans. Biomed. Eng.* **63** 111–9

[47] Massey T L, Santacruz S R, Hou J F, Pister K S J, Carmena J M and Maharbiz M M 2019 A high-density carbon fiber neural recording array technology *J. Neural Eng.* **16** 016024

[48] Hejazi M A, Tong W, Stacey A, Soto-Breceda A, Ibbotson M R, Yunzab M, Maturana M I, Almasi A, Jung Y J, Sun S, Meffin H, Fang J, Stamp M E M, Ganesan K, Fox K, Rifai A, Nadarajah A, Falahatdoost S, Prawer S, Apollo N V and Garrett D J 2020 Hybrid diamond/ carbon fiber microelectrodes enable multimodal electrical/chemical neural interfacing *Biomaterials* **230** 119648

[49] Marshall S P, Lin W, Patel P R, Shih A J and Chestek C A 2016 Effects of geometry and material on the insertion of very small neural electrode *2016 38th Annual International Conference of the IEEE Engineering in Medicine and Biology Society (EMBC)* pp 2784–8

[50] Liu J, Fu T-M, Cheng Z, Hong G, Zhou T, Jin L, Duvvuri M, Jiang Z, Kruskal P, Xie C, Suo Z, Fang Y and Lieber C M 2015 Syringe-injectable electronics *Nat. Nanotechnol.* **10** 629–636–629–636

[51] Zhao Z, Li X, He F, Wei X, Lin S and Xie C 2019 Parallel, minimally-invasive implantation of ultra-flexible neural electrode arrays *J. Neural Eng.* **16** 035001

[52] Takmakov P, McKinney C J, Carelli R M and Wightman R M 2011 Instrumentation for fast-scan cyclic voltammetry combined with electrophysiology for behavioral experiments in freely moving animals *Rev. Sci. Instrum.* **82** 74302

[53] Robinson D L and Wightman R M 2006 *Electrochemical methods for neuroscience* ed A C Michael and L M Borland

[54] Bucher E S, Brooks K, Verber M D, Keithley R B, Owesson-white C, Carroll S, Takmakov P, Mckinney C J and Wightman R M 2013 Flexible Software Platform for Fast-Scan Cyclic Voltammetry Data Acquisition and Analysis *Anal. Chem.* **85** 10344–53

[55] Gittins R and Harrison P J 2004 Neuronal density, size and shape in the human anterior cingulate cortex: a comparison of Nissl and NeuN staining *Brain Res. Bull.* **63** 155–60

[56] Schindelin J, Arganda-Carreras I, Frise E, Kaynig V, Longair M, Pietzsch T, Preibisch S, Rueden C, Saalfeld S, Schmid B, Tinevez J-Y, White D J, Hartenstein V, Eliceiri K, Tomancak P and Cardona A 2012 Fiji: an open-source platform for biological-image analysis *Nat. Methods* **9** 676–82

[57] Taylor I M, Robbins E M, Catt K A, Cody P A, Happe C L and Cui X T 2017 Enhanced dopamine detection sensitivity by PEDOT/graphene oxide coating on in vivo carbon fiber electrodes *Biosens. Bioelectron.* **89** 400–10

[58] Vreeland R F, Atcherley C W, Russell W S, Xie J Y, Lu D, Laude N D, Porreca F and Heien M L 2015 Biocompatible PEDOT:Nafion Composite Electrode Coatings for Selective Detection of Neurotransmitters in Vivo *Anal. Chem.* **87** 2600–7

[59] Buzsáki G 2004 Large-scale recording of neuronal ensembles *Nat. Neurosci.* **7** 446–51

[60] Robinson D L, Heien M L A V and Wightman R M 2002 Frequency of Dopamine Concentration Transients Increases in Dorsal and Ventral Striatum of Male Rats during Introduction of Conspecifics *J. Neurosci.* **22** 10477–86

[61] Beier K T, Steinberg E E, DeLoach K E, Xie S, Miyamichi K, Schwarz L, Gao X J, Kremer E J, Malenka R C and Luo L 2015 Circuit Architecture of VTA Dopamine Neurons Revealed by Systematic Input-Output Mapping *Cell* **162** 622–34

[62] Ward M P, Rajdev P, Ellison C and Irazoqui P P 2009 Toward a comparison of microelectrodes for acute and chronic recordings *Brain Res.* **1282** 183–200

[63] Gillis W F, Lissandrello C A, Shen J, Pearre B W, Mertiri A, Deku F, Cogan S, Holinski B J, Chew D J, White A E, Otchy T M and Gardner T J 2018 Carbon fiber on polyimide ultra-microelectrodes *J. Neural Eng.* **15** 016010

[64] Gerwig R, Fuchsberger K, Schroeppel B, Link G S, Heusel G, Kraushaar U, Schuhmann W, Stett A and Stelzle M 2012 PEDOT–CNT Composite Microelectrodes for Recording and Electrostimulation Applications: Fabrication, Morphology, and Electrical Properties *Front. Neuroeng.* **5** 1–11

[65] Luo X, Weaver C L, Zhou D D, Greenberg R and Cui X T 2011 Highly stable carbon nanotube doped poly (3 ,4-ethylenedioxythiophene) for chronic neural stimulation *Biomaterials* **32** 5551–7

[66] Vitale F, Vercosa D G, Rodriguez A V., Pamulapati S S, Seibt F, Lewis E, Yan J S, Badhiwala K, Adnan M, Royer-Carfagni G, Beierlein M, Kemere C, Pasquali M and

Robinson J T 2018 Fluidic Microactuation of Flexible Electrodes for Neural Recording *Nano Lett.* **18** 326–35

[67] Vitale F, Summerson S R, Aazhang B, Kemere C and Pasquali M 2015 Neural stimulation and recording with bidirectional, soft carbon nanotube fiber microelectrodes *ACS Nano* **9** 4465–74

[68] Weiss H R, Buchweitz E, Murtha T J and Auletta M 1982 Quantitative regional determination of morphometric indices of the total and perfused capillary network in the rat brain. *Circ. Res.* **51** 494–503

[69] Lu C W, Patil P G and Chestek C A 2012 Current Challenges to the Clinical Translation of Brain Machine Interface Technology *Int. Rev. Neurobiol.* **107** 137–60

[70] McCallum G A, Sui X, Qiu C, Marmerstein J, Zheng Y, Eggers T E, Hu C, Dai L and Durand D M 2017 Chronic interfacing with the autonomic nervous system using carbon nanotube (CNT) yarn electrodes *Sci. Rep.* **7** 11723

[71] Berke J D 2018 What does dopamine mean? *Nat. Neurosci.* **21** 787–93

[72] Aragona B J, Day J J, Roitman M F, Cleaveland N A, Mark Wightman R and Carelli R M 2009 Regional specificity in the real-time development of phasic dopamine transmission patterns during acquisition of a cue-cocaine association in rats *Eur. J. Neurosci.* **30** 1889–99

[73] Threlfell S, Lalic T, Platt N J, Jennings K A, Deisseroth K and Cragg S J 2012 Striatal Dopamine Release Is Triggered by Synchronized Activity in Cholinergic Interneurons *Neuron* **75** 58–64

[74] Cachope R, Mateo Y, Mathur B N, Irving J, Wang H-L, Morales M, Lovinger D M and Cheer J F 2012 Selective Activation of Cholinergic Interneurons Enhances Accumbal Phasic Dopamine Release: Setting the Tone for Reward Processing *Cell Rep.* **2** 33–41

[75] Mohebi A, Pettibone J R, Hamid A A, Wong J-M T, Vinson L T, Patriarchi T, Tian L, Kennedy R T and Berke J D 2019 Dissociable dopamine dynamics for learning and motivation *Nature* **570** 65–70

[76] Panin F, Cathala A, Piazza P V and Spampinato U 2012 Coupled intracerebral microdialysis and electrophysiology for the assessment of dopamine neuron function in vivo *J. Pharmacol. Toxicol. Methods* **65** 83–92

[77] Guitchounts G and Cox D 2020 64-Channel Carbon Fiber Electrode Arrays for Chronic Electrophysiology *Sci. Rep.* **10** 3830

[78] Wickersham I R, Lyon D C, Barnard R J O, Mori T, Finke S, Conzelmann K-K, Young J A T and Callaway E M 2007 Monosynaptic Restriction of Transsynaptic Tracing from Single, Genetically Targeted Neurons *Neuron* **53** 639–47

[79] Cai D, Cohen K B, Luo T, Lichtman J W and Sanes J R 2013 Improved tools for the Brainbow toolbox *Nat. Methods* **10** 540

[80] Livet J, Weissman T A, Kang H, Draft R W, Lu J, Bennis R A, Sanes J R and Lichtman J W 2007 Transgenic strategies for combinatorial expression of fluorescent proteins in the nervous system *Nature* **450** 56

[81] Roossien D H and Cai D 2017 Imaging Neural Architecture in Brainbow Samples *Site-Specific Recombinases: Methods and Protocols* ed N Eroshenko (New York, NY: Springer New York) pp 211–28

[82] Roossien D H, Webb J M, Sadis B V, Yan Y, Min L Y, Dizaji A S, Bogart L J, Mazuski C, Huth R S, Stecher J S, Lichtman J W, Hensch T K, Herzog E D and Cai D 2017 Neuronal tracing and analysis by multispectral tracing in densely labeled mouse brain

bioRxiv 230458

[83] Sümbül U, Roossien D, Cai D, Chen F, Barry N, Cunningham J P, Boyden E and Paninski L 2016 Automated scalable segmentation of neurons from multispectral images *Advances in Neural Information Processing Systems 29* ed D D Lee, M Sugiyama, U V Luxburg, I Guyon and R Garnett (Curran Associates, Inc.) pp 1912–20

[84] Tillberg P W, Chen F, Piatkevich K D, Zhao Y, Yu C-C (Jay), English B P, Gao L, Martorell A, Suk H-J, Yoshida F, DeGennaro E M, Roossien D H, Gong G, Seneviratne U, Tannenbaum S R, Desimone R, Cai D and Boyden E S 2016 Protein-retention expansion microscopy of cells and tissues labeled using standard fluorescent proteins and antibodies *Nat. Biotechnol.* **34** 987